Modeling and Box-Behnken Design Optimization for the Efficient Removal of Ibuprofen via Heterogeneous Fenton-Like Reactions Using a Fe3O4/HNTs as a Catalyst

Erick A. García-García , Adolfo E. Obaya-Valdivia , Jaime Jiménez-Becerril , Julio C. Morales-Mejía , José A. Chávez-Carvayar , Yolanda M. Vargas-Rodríguez *

Posted Date: 15 April 2026

doi: 10.20944/preprints202604.1141.v1

Keywords: ibuprofen; fenton-like; Box Benken design; mineralization; adsorption; magnetite; halloysite nanotubes

 doi:10.20944/preprints202604.1141.v1

Article

Modeling and Box-Behnken Design Optimization for the Efficient Removal of Ibuprofen via Heterogeneous Fenton-Like Reactions Using a Fe_3O_4/HNTs as a Catalyst

Erick A. García-García [1], Adolfo E. Obaya-Valdivia [1], Jaime Jiménez-Becerril [2], Julio C. Morales-Mejía [3], José A. Chávez-Carvayar [4] and Yolanda M. Vargas-Rodríguez [1,*]

[1] Laboratorio de Nanomateriales y Catálisis. FES Cuautitlán, Universidad Nacional Autónoma de México. Estado de México, México. Avenida 1° de mayo s/n, Sta Maria Guadalupe las Torres, 54740. Estado de México, México

[2] Departamento de Química. Instituto Nacional de Investigaciones Nucleares. Carretera México-Toluca s/n, La Marquesa, Ocoyoacac, C.P. 52750. Estado de México, México

[3] Department of Engineering and Technology, FES Cuautitlán, National Autonomous University of Mexico, 1o May Avenue S/N, Sta Maria Guadalupe las Torres, 54740. Estado de México, México

[4] Instituto de Investigaciones en Materiales, Universidad Nacional Autónoma de México. Circuito Exterior, Investigación Científica S/N, C.U., 04510 Ciudad de México, CDMX. México

* Correspondence: ymvargas@unam.mx (Y.M.V.-R.); garciag.eaxel@gmail.com (E.A.G.-G.).

Abstract

A Fe_3O_4/HNTs composite was synthesized, characterized by XRD, FTIR, SEM, and N_2 adsorption-desorption, and was used for an ibuprofen adsorption and oxidation study. The response surface methodology (RSM) and Box-Behnken experimental designs were used. The effect of pH, contact time, IBU concentration, and Fe_3O_4/HNTs dosage on ibuprofen adsorption were evaluated. Additionally, adsorption isotherms and a kinetic study were performed. The effect of pH, H_2O_2 concentration, and Fe_3O_4/HNTs dosage for IBU oxidation were also studied. The results of ibuprofen adsorption on Fe_3O_4/HNTs indicate that adsorption was favored at acidic pH. The adsorption followed pseudo-second-order kinetics and a Freundlich isotherm. A 99.99% IBU oxidation and 99% mineralization were achieved at pH 7, Fe_3O_4/HNTs dosage of 1.5 g L^{-1}, and 0.5 M H_2O_2. The Fe_3O_4/HNTs catalyst prepared in this study was efficient in removing aqueous ibuprofen through heterogeneous Fenton-like reaction.

Keywords: ibuprofen; fenton-like; Box Benken design; mineralization; adsorption; magnetite; halloysite nanotubes

1. Introduction

Chemicals of Emerging Concern (CECs) are chemicals recently identified as threats to the environment and human health that require extensive regulation or monitoring [1]. These compounds include pharmaceuticals, industrial chemicals, personal care products, and others that can harm both aquatic and terrestrial ecosystems as well as human health [2]. CECs are often released into the environment through human activities, such as pharmaceutical use, industrial production, and consumer products [3]. Unlike conventional pollutants, which have been studied and regulated for decades, CECs pose additional challenges due to their dynamic nature and the lack of comprehensive data on their long-term effects [4]. For instance, ibuprofen (IBU) is a widely used nonsteroidal anti-inflammatory drug (NSAID) known for its analgesic and antipyretic properties. It is commonly prescribed to relieve fever, pain, rheumatoid arthritis, and osteoarthritis [5]. IBU is

 doi:10.20944/preprints202604.1141.v1

consumed extensively in both human and veterinary medicine [6], and it is the third most widely used drug in the world, with an annual consumption of nearly 200 tons [7]. IBU has been found in water treatment plants in Australia, Canada, Chile, China, Finland, Ghana, Greece, India, Japan, Korea, Mexico, New Zealand, Palestine, Poland, Portugal, South Africa, Singapore, Spain, Switzerland, Thailand, Turkey, United Arab Emirates, United Kingdom, United States, and Vietnam [8,9]. It has also been detected in domestic wastewater in Spain, Denmark, Singapore, the Czech Republic, Germany, the United Kingdom, Sweden, and Mexico [10–19], and in surface water bodies such as the Madín Dam in Mexico [20,21]. Its presence is primarily due to human and animal excretion and its introduction through wastewater treatment systems. Its removal in wastewater treatment plants (WWTPs) is limited, which favors its release into the environment [7]. This situation is further exacerbated by animal excretion, the disposal of expired medications, and the discharge of untreated water.

IBU has been reported to have several adverse effects on organisms, including cellular and genetic damage to the freshwater bivalve *Dreissena polymorpha*, delayed hatching of eggs in the freshwater fish *Oryzias latipes* and freshwater cladocerans such as *Daphnia magna* and *Moina macrocopa*, inhibition of photosynthesis in the freshwater diatom *Navicula sp.*, damage to the hemocytes of *Ruditapes philippinarum*, and an impact on the growth of the freshwater microalga *Scenedesmus rubescens* [22–26].

IBU has been removed by methods such as adsorption with different materials, including biochar [6], carbon nanotube-based materials [27], nanoparticles with polyamidoamine [28], and magnetic nanoparticles such as Fe_3O_4@hydroxyapatite [29]; biological methods [30,31]; and advanced oxidation processes (AOPs). AOPs refer to a group of chemical treatment processes designed to remove organic and inorganic contaminants from water and wastewater. These processes are typically based on the generation of highly reactive hydroxyl radicals (·OH), which can break down a wide range of pollutants [32].

One of the most well-known AOPs is the Fenton process, which is based on the generation of hydroxyl radicals from the decomposition of hydrogen peroxide (H_2O_2) in the presence of materials containing Fe (II) ions under acidic conditions. This reaction yields hydroxyl radicals (•OH) and Fe (III). Additionally, these ferric ions react with hydrogen peroxide, producing hydroperoxyl radicals (•OOH) and regenerating the catalyst (ferrous ions). If the reaction is initiated by Fe (III) ions, the process is commonly referred to as "Fenton-like." However, there is a redox cycle that creates a series of redox reactions, causing both species to be present simultaneously, regardless of the starting ion [32].

IBU has been oxidized through the Fenton process and its various combinations with different sources of iron and other materials, such as sonolysis and sono-Fenton systems with Fe(II) ions, homogeneous modified Fenton-like oxidation with an FeIII-gallic acid complex, heterogeneous Fenton with Fe-zeolite catalysts, plasma-supported Fenton (with Fe-based ordered mesoporous carbon; 88.3% efficiency), electro-Fenton systems, Fenton-like with zero-valent ions, and electro-Fenton with zero-valent ions [35–40].

Among ion-based materials, Fe_3O_4 is one of the most reported iron(III) compounds for Fenton-like oxidation studies of IBU [41,42]. Heterogeneous photo-Fenton processes include carbon dots/Fe3O4@carbon sphere pomegranate-like composites activated by a persulfate system, heterogeneous photo-Fenton with humic acid-coated Fe3O4, sono-electrolytic Fenton, Fe_3O_4 supported on multi-walled carbon nanotubes (MWCNTs), and the Fenton-like graphene oxide-based electro-Fenton process [41–46].

Halloysite nanotubes (HNTs) are an economically viable material that can be used without further purification. HNTs are clay minerals from the kaolin group, typically composed of two layers rolled into a tubular morphology. The outer layer is composed of silicates (tetrahedral crystals), whereas the inner layer of the nanotube consists of alumina (Al_2O_3) octahedra. Due to their large surface area, HNTs are known to be good adsorbents and catalyst supports [47–50].

 doi:10.20944/preprints202604.1141.v1

In the present study, the elimination of IBU from aqueous solutions was achieved through both adsorption onto Fe_3O_4//HNTs and heterogeneous Fenton oxidation using Fe_3O_4//HNTs as a catalyst. Magnetite particles were synthesized in situ on halloysite nanotubes through the coprecipitation method. This composite material was suitable for supported-catalyst development due to its proper distribution and stability in suspensions, as well as its magnetic properties, which allow for better recovery under an external magnetic field.

Fe_3O_4/HNTs were characterized by XRD, FTIR, SEM and N_2 adsorption-desorption analysis. Response surface methodology (RSM) with 2 factors (adsorbent dose and pH) was applied to study IBU removal from aqueous solution by adsorption using Fe_3O_4/HNTs. The experimental design, determination of the coefficients, data analysis, and graph generation were conducted using Design-Expert® version 11.

The initial IBU concentration was maintained at 15 mg L^{-1} throughout all experiments. Subsequently, a Box–Behnken experimental design was implemented to develop a mathematical model for predicting the optimal operating conditions for IBU oxidation at this concentration using Fe_3O_4/HNTs as the catalyst. The initial pH, H_2O_2 concentration, and Fe_3O_4/HNTs dosage were considered as the factors. According to the results obtained from the experimental design for IBU oxidation, the heterogeneous Fenton-like process conducted under the optimized conditions yielded the highest IBU removal efficiency.

2. Materials and Methods

2.1. Preparation of Fe_3O_4/HNTs Composite

Halloysite nanotubes $Al_2Si_2O_5(OH)_4 \cdot 2\ H_2O$ (HNTs), iron(III) chloride hexahydrate ($FeCl_3\ 6H_2O$) and iron sulfate heptahydrate ($FeSO_4 \cdot 7H_2O$) and ammonium hydroxide solution (NH_4OH, 28-30%), hydrogen peroxide solution (H_2O_2, 30% w/w), solutions of hydrochloric acid (HCl, 0.1 M) and sodium hydroxide (NaOH, 0.1 M) were purchased from Sigma-Aldrich. The catalyst (Fe_3O_4/HNTs) was synthesized using a coprecipitation method using Fe(ll) and Fe(lll) salts in a basic medium in the presence of HNTs as described by Maleki and Sadati [51]. The HNTs and distilled water were added to the 3-neck flask and kept under constant stirring at 60°C. Then, $FeSO_4 \cdot 7H_2O$ and $FeCl_3 \cdot 6H_2O$ were solubilized in distilled water and added to the 3-neck flask. The solution was kept under constant stirring at 60°C for 1 hour. Afterward, NH_4OH was slowly added the pH reached 11,, maintaining stirring, at 70 °C for 2 hours. The resulting solution was stored at room temperature for 24 hours, forming solid deposition. Neodymium magnets were used to hold solids along with the supernatant liquid. Solids were washed several times with distilled water until wash-water had pH 7. The solid was dried at 70 °C for two days and crushed with a mortar until a fine powder was obtained.

2.2. Characterization of the Catalyst

The HNTs, magnetite, and solid catalyst were characterized using various techniques. The morphology and particle size were determined by scanning electron microscopy (JEOL-6460LV at 20 kV; JEOL, Inc., U.S.) and energy dispersive X-ray spectroscopy (EDX). The specific surface area of the samples was determined using the Brunauer-Emmett-Teller (BET) method. The Barrett-Joyner-Halenda (BJH) method at 77 K (Autosorb 1 MP, Quantachrome Instruments) was used to estimate pore volume and pore size distribution. Before measurements, the samples were degassed under vacuum at 573 K for 10 hours. The crystalline phases were identified by X-ray diffraction (XRD) using a Bruker AXS X-ray diffractometer (D8 Advanced Plus, with CuKa1 monochromatic radiation, λ = 1.54056 Å). Data collection was performed in the 2θ range from 2° to 70°, with a step width of 0.02° and a count time per step of 1.8 seconds. Normal operating conditions were 35 kV and 30 mA. Infrared spectra were obtained using a Fourier-transform infrared (FT-IR) spectrometer (Nicolet 6700 with Ge-on KBr beamsplitter, Thermo Scientific), and the amount of IBU adsorbed onto the catalyst particles was determined using a Perkin Elmer 283 spectrometer (KBr tablets) in the wavenumber range from 400 to 4000 cm^{-1}.

 doi:10.20944/preprints202604.1141.v1

2.3. Adsorption

The Fe_3O_4/HNTs were then separated using an external magnet. A UV–visible spectrophotometer (UV-Vis Perkin Elmer Model Lambda 25) was used to determine the IBU concentration in solution. In the calibration curve of ibuprofen in an aqueous medium, the absorbance spectra were plotted as a function of wavelength in the 200-300 nm range for concentrations of 1.5 to 15 mg L^{-1}. Previously, the spectra were carried out at pH 2, 7, and 12, where it is observed that the wavelength of maximum absorption for solutions at pH 2 is 222 nm and 224 nm for IBU solutions at pH 7 and 12, respectively. The amount of IBU adsorbed was calculated by the difference between the initial concentration and the equilibrium concentration of IBU; it was calculated as follows (Equation 1). IBU solutions were prepared in deionized water. The pH was then adjusted using either HCl (0.1 M) or NaOH (0.1 M). The solutions were continuously stirred at 293.15 K for 24 hours. The Fe3O4/HNTs were then separated using an external magnet. A UV–visible spectrophotometer (UV-Vis Perkin Elmer Model Lambda 25) was used to determine the IBU concentration in the solution. For the calibration curve of ibuprofen in an aqueous medium, the absorbance spectra were plotted as a function of wavelength in the 200-300 nm range for concentrations ranging from 1.5 to 15 mg L^{-1}. The spectra were previously recorded at pH 2, 7, and 12, where it was observed that the wavelength of maximum absorption for solutions at pH 2 was 222 nm, and for IBU solutions at pH 7 and 12, it was 224 nm, respectively. The amount of IBU adsorbed by the adsorbent at any time, q_t(mg g^{-1}), and at equilibrium, q_e(mg g^{-1}) respectively was calculated based on the concentration in the solution before and after adsorption, according to Equations 1 and 2. The amount of IBU adsorbed by Fe_3O_4/HNTs at any time, q_t(mg g^{-1}), and at equilibrium, q_e(mg g^{-1}), was calculated based on the concentration in the solution before and after adsorption, using Equations 1 and 2.

$$q_t = \frac{(Co-Ce)V}{W} \quad (1)$$

$$q_e = \frac{(Co-Ct)V}{W} \quad (2)$$

where C_0(mg L^{-1}) is the initial IBU concentration, C_t(mg L^{-1}) is the concentration after a contact time t, C_e(mg L^{-1}) is the remaining concentration at equilibrium, V(L) is the sample volume, and W(mg) is the mass of Fe_3O_4/HNTs used in each test.

The percentage of IBU adsorption onto Fe_3O_4/HNTs was calculated using Equation 3.

$$IBU\ adsorbed\ (\%) = \frac{Co-Cf}{Co} * 100\% \quad (3)$$

where C_o is the initial concentration of IBU (15 mg L^{-1}) and C_f is the final concentration of IBU after adsorption.

The adsorption results were fitted with pseudo-first order (PFO) kinetic, pseudo-second order (PSO) kinetic, and intra-particle diffusion were fitted to determine the adsorption mechanisms.

This PFO kinetic model (Equation 4) was analyzed because it typically applies to physisorption processes and describes physical interactions between the adsorbate and the adsorbent, such as Van der Waals or dipole–dipole forces. In this model, q_t and q_e (mg g^{-1}) represent the amounts of IBU adsorbed at time t and at equilibrium, respectively; t (min) is the adsorption time, and k_1 (min^{-1}) is the Lagergren pseudo-first-order rate constant [52].

$$Ln\ (q_e - q_t) = q_e - k_1 t \quad (4)$$

The pseudo-second order (PSO) kinetic model Equation (5). This model implies that the adsorbent surface exhibits a specific affinity for the adsorbate, and that the active sites progressively become saturated over time, which gradually reduces the adsorption rate until equilibrium is reached. Where, q_t and q_e (mg g^{-1}) represent the amounts of IBU adsorbed at time t and at equilibrium, respectively; t (min) is the adsorption time, and k_2 (mg g^{-1} min^{-1}) is the pseudo-second-order rate constant [53].

$$t/q_t = 1/k_2 q_e^2 + 1/q_e\, t \quad (5)$$

 doi:10.20944/preprints202604.1141.v1

The intraparticle diffusion model (Equation 6) posits that the adsorption rate is, at least in part, governed by the transport of the adsorbate from the bulk solution into the internal pores of the adsorbent. This internal diffusion takes place through the porous structure of the solid and may become the rate-limiting step when active sites are not readily accessible from the external surface, due to the adsorbent's pore characteristics. In this model, q_t is the amount of IBU adsorbed at time t (min), k_i is the intraparticle diffusion rate constant (mg g^{-1} $min^{1/2}$), and C is a constant (mg g^{-1}) associated with the boundary layer thickness [54].

$$q_t = k_i t^{1/2} + C \quad (6)$$

The adsorption isotherm data were obtained at 298.15 K. The concentration range is 5–15 mg L^{-1}. Adsorption equilibrium data were analyzed using the Henry, Freundlich and Langmuir isotherms models.

Henry's isotherm, Equation (7), assumes ideal behavior, where adsorption occurs monolayer without interactions between adsorbed molecules and no saturation of adsorption sites. Although simple, the Henry isotherm is fundamental for understanding adsorption at low coverage and is often used to define the initial slope of more complex isotherms, such as Freundlich or Langmuir [55].

$$q_e = K_H C_e \quad (7)$$

The Freundlich isotherm shown in the Equation 8, is an empirical model that can be applied to multilayer adsorption, with a non-uniform distribution of the heat of adsorption and affinities on the heterogeneous surface, is an empirical model that can be applied to multilayer adsorption, with a non-uniform distribution of the heat of adsorption and affinities on the heterogeneous surface [56]. Where qe (mg·g^{-1}) is the equilibrium amount of adsorbed IBU, Ce (mg·L^{-1}) is the equilibrium concentration of IBU, and K_F (mg·g^{-1}) and n are constants for a given adsorbate and adsorbent, per mass unit of adsorbent, at equilibrium.

$$\log q_e = \log K_F + \left(1/n\right) \log C_e \quad (8)$$

The Langmuir isotherm, as expressed in Equation 9, assumes that adsorption occurs as a monolayer on a homogeneous surface. In this context, Ce (mg·L^{-1}) represents the equilibrium concentration of the adsorbate in the solution phase, while qe (mg·g^{-1}) denotes the amount of adsorbate retained per unit mass of adsorbent when equilibrium is reached. The parameters q_0 and K_L are the Langmuir constants, which describe the maximum adsorption capacity and the affinity of the binding sites, respectively [57].

$$C_e/q_e = \left(1/q_{max} K_L\right) + (1/q_o) C_e \quad (9)$$

2.4. Ibuprofen Oxidation by Heterogeneous Fenton Reaction

IBU oxidation was carried out in propylene centrifuge tubes. Solutions of 15 mg L^{-1} were prepared in deionized water, and the pH was adjusted using either HCl (0.1 M) or NaOH (0.1 M). After pH adjustment, the corresponding dose of Fe_3O_4/HNTs were mixed with 10 mL of IBU solution. The addition of hydrogen peroxide initiated the heterogeneous Fenton-type reaction. After 24 h of reaction, the catalyst was separated with a magnet from the reaction samples. A sample of the supernatant liquid was immediately collected, and the chemical oxygen demand (COD) was determined. Digester equipment for COD vials HI 83980 Hanna was used for the COD. An UV–visible spectrophotometer (UV-Vis Perkin Elmer Model Lambda 25) was used to determine the Cr^{3+} and Cr^{6+} (as dichromate) absorbance in digested samples to match them against the corresponding COD calibration plot.

2.5. Response Surface Methodology and Experimental Design

For the adsorption and oxidation studies, Box-Behnken experimental designs were employed. pH, dosage (adsorbent/catalyst), and H_2O_2 concentration were selected as independent variables. These factors were evaluated at two levels and a center point (-1, 0, and +1).

 doi:10.20944/preprints202604.1141.v1

A second order (quadratic) model was obtained to analyze the interactions between variables (Eq. 10). An analysis of variance (ANOVA) was applied to verify the statistical significance of the model terms.

$$Y = \beta_o + \beta_1 X_1 + \beta_2 X_2 + \beta_{12} X_1 X_2 + \beta_{11} X_1^2 + \beta_{22} X_2^2 \quad (10)$$

where X_i, X_i^2, and $X_i X_j$ represent the linear, quadratic, and interaction terms, respectively. β_0, β_{ii}, and β_{ij} are the coefficients of the linear model terms, the quadratic model terms, and the interaction terms, respectively, and Y represents the response, which is the percentage of adsorption and mineralization respectively. *Design Expert version 11* (Stat-Ease, Inc) was the software used. Response surface methodology (RSM) was used as a statistical and mathematical approach to model and analyze adsorption and oxidation processes where multiple variables influence the desired outcome, to optimize the response [58].

2.6. Mineralization of Ibuprofen

Based on the results obtained in the design of experiments for IBU mineralization, a heterogeneous Fenton-type reaction was carried out under the optimal reaction conditions in which more significant IBU mineralization is obtained. The IBU concentration was measured before and after the heterogeneous Fenton reaction using gas chromatography coupled to a mass spectrometer (ACQUITY UPLC H-Class), with an ACQUITY UPLC BEH C18 column, 1.7 µm, 2.1 mm x 50 mm, mobile phase A: 100% Milli Q Water, Mobile phase B: 100% UPLC Acetonitrile, Flow Rate: 0.3 mL/min, Injection Volume: 10 µL, Running Time: 5 minutes Wavelength, PDA detector: 210-600 nm, Column temperature: 30°C. A calibration curve was performed using IBU at concentrations of 2.5, 5, 10, and 15 mgL^{-1}, and the mass spectrum for ibuprofen was obtained.

3. Results

3.1. Characterization of the Catalyst

The morphology and size details of the Fe_3O_4/HNTs catalyst were determined by SEM. Figure 1 indicates that the catalyst particles were nearly spherical and with uniform size; in addition, halloysite nanotubes exhibited irregular needle shape and irregular agglomerations on and around catalyst particles. It might be due to strong inter-particle Van der Waals forces or due to magnetic attraction among the Fe_3O_4 nanoparticles. Also, SEM images confirm the catalyst's sized structure and morphology. Chemical composition of catalyst, determined by EDX, confirms the presence of carbon, oxygen, silicon, aluminum, and sulfur elements

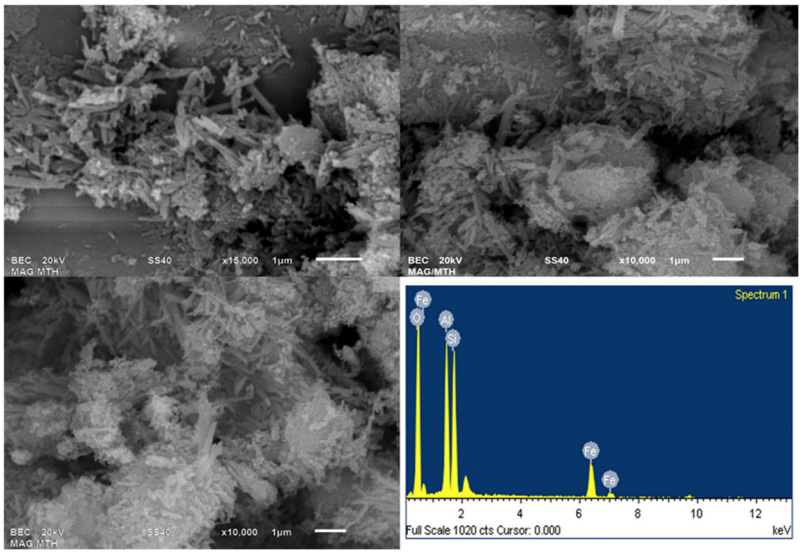

Figure 1. SEM image and the EDX image of Fe_3O_4/HNTs.

 doi:10.20944/preprints202604.1141.v1

The pore size distribution of the Fe_3O_4, HNTs, and Fe_3O_4/HNTs samples was obtained using the Barret-Joyner-Hallenda (BJH) method [59]. In all cases, mesoporous particles (2 - 50 nm) and macroporous particles with a pore diameter greater than 50 nm [60]. The pore size distribution for halloysite is trimodal, with maximums at 3.3, 11, and 75 nm, respectively. The pore size distribution for magnetite is monomodal, with a maximum of 7.7 nm. The Fe_3O_4/HNTs catalyst presents a bimodal pore size distribution with maxima at 3.3 and 18 nm. From nitrogen adsorption-desorption study for halloysite, magnetite, and magnetite/halloysite samples (Figure 2a), it is observed that the three samples presented hysteresis cycles, indicating the presence of mesoporous material. For HNTs, a minimal hysteresis cycle of type H3 is observed, characteristic of mesoporous materials that form agglomerates of particles with pores or a slit-lamellar shape with non-uniform size, characteristic of mesoporous materials that form agglomerates of particles with pores or a slit-lamellar shape with non-uniform size [60], and that has been observed in different HNTs samples [61]. Fe_3O_4 and Fe_3O_4/HNTs samples show H1-type hysteresis cycles, which are characteristic of solids consisting of particles crossed by almost cylindrical channels or formed by aggregates (consolidated) or agglomerates (unconsolidated) of spheroidal particles with pores of size and uniform shape [60].The similarity of the types of hysteresis between Fe_3O_4 and Fe_3O_4/HNTs indicates a higher magnetite content in the catalyst than halloysite. The specific surface area of Fe_3O_4, HNTs, and Fe_3O_4/HNTs was determined using the BET equation, using the results of N_2 adsorption on the surfaces. The BET area for Fe_3O_4/HNTs was 67.7 $m^2\ g^{-1}$; it was higher than the area of the HNTs (34.4 $m^2\ g^{-1}$) because the magnetite is heterogeneously supported on the halloysite, generating greater dispersion between the molecules, preventing them from agglomerating, due to this the Fe_3O_4/HNTs has a greater dispersion and a greater surface area than HNTs.

The X-ray diffraction pattern of the Fe_3O_4/HNTs sample is shown in Figure 2b). The crystalline phases identified are magnetite and HNTs according to the Power Diffraction Pattern sheets (PDF) 01-076-0958 and 00-009-0451, respectively. The HNTs were identified with the reflections near at 2θ (11.87°, 20.1°, 24.5°, 35.1°, 38.1°, 54.6° and 62.6°). The most important result marks this identification for d_{001}, corresponding to the reflection at 11.87°, which was observed in the pattern. This reflection corresponds to a *d* space around 7.77 Å, a characteristic result for dehydrated HNTs (7 Å) [62,63]. The magnetite phase was identified with the reflections at 2θ (30.11°, 35.46°, 43.1°, 57.0°, and 62.59°). The most important result marks this identification for $d_{220,}$ corresponding to the reflection at 30.11° observed in the pattern. The crystalline domain size (D) was determined using the Scherrer equation. The highest intensity reflections for HNTs and Fe_3O_4 were selected in the X-ray diffraction pattern of the Fe_3O_4/HNTs sample. The crystalline domain size (D) was determined using the Scherrer equation. The highest intensity reflections for HNTs and Fe_3O_4 were selected in the X-ray diffraction pattern of the Fe_3O_4/HNTs sample. The crystallite sizes of the natural HNTs and the magnetite synthesized by the coprecipitation method were 13 and 12 nm, respectively. However, when the synthesis of Fe_3O_4 was carried out in the presence of HNTs, the crystallite size of both HNTs and Fe_3O_4 increased to 25 nm and 40 nm, respectively.

 doi:10.20944/preprints202604.1141.v1

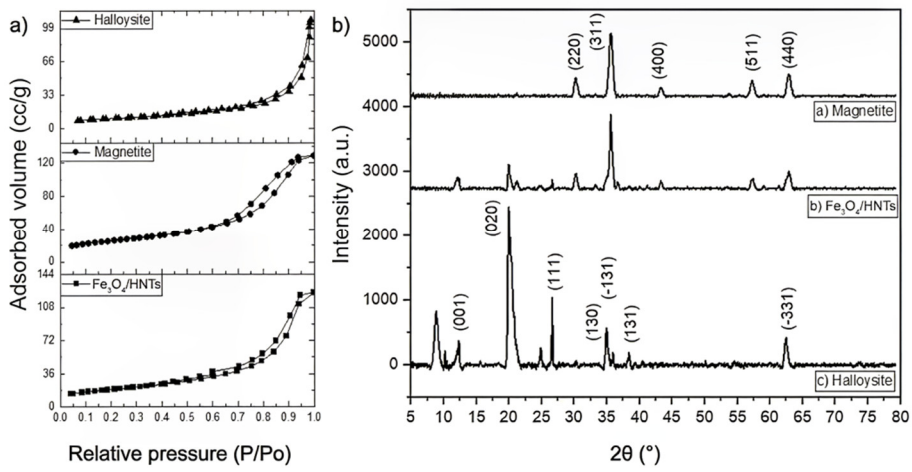

Figure 2. a) Hysteresis loops: H3-type for HNTs, H1-type for Fe_3O_4 and Fe_3O_4/HNTs; b) X-ray diffraction pattern of magnetite, Fe_3O_4/HNTs, and HNTs.

3.2. Box-Behnken Design for the Adsorption of Ibuprofen on Fe_3O_4/HNTs

A design was implemented to evaluate the factors used (A: pH, and B: Fe_3O_3/HNT) and determine their effect on the adsorption of IBU onto Fe_3O_3/HNT. Three levels were evaluated for each factor (-1, +1, and 0) (Table 1). In addition to three center points, resulting in a total of 12 experiments where the percentage of adsorption was measured in each one (Table 2).

Table 1. Code and levels of Box-Behnken design for the adsorption of IBU on Fe_3O_4/HNTs.

Factor	Code	Low level (-1)	Central point	Low level (+1)
pH	X1=A	2	7	12
Adsorbent dose (g L^{-1})	X2=B	0.5	1.5	2.5

Table 2. Amount of IBU adsorbed on Fe_3O_4/HNTs.

Run	Fe_3O_4/HNTs (g L-1)	pH	Adsorbed IBU (%)
1	0.5	2	7.85
2	0.5	7	2.94
3	0.5	12	1.86
4	1.5	2	10.06
5	1.5	7	3.13
6	1.5	12	2.56
7	2.5	2	8.51
8	2.5	7	3.22
9	2.5	12	2.04
10	1.5	7	3.29
11	1.5	7	3.37
12	1.5	7	3.42

The statistical models, shown in Table 3, were obtained using the Design Expert 11 software. The quadratic model best fits the adsorption results, considering different pH values and doses of the

 doi:10.20944/preprints202604.1141.v1

adsorbent. P-values less than 0.0500 indicate model terms are significant in this case A, A2, B2 are significant model terms. Values greater than 0.1000 indicate the model terms are not significant.

Table 3. Lack-of-fit test of the optimization models for the adsorption of IBU onto Fe_3O_4/HNTs.

Source	Sequential p-value	Lack of fit p-value	Adjusted R^2	Predicted R^2
Linear	0.0009	0.0006	0.7401	0.6220
2FI	0.8766	0.0005	0.7085	0.4662
Quadratic	0.0004	0.0122	0.9721	0.8767
Cubic	0.3341	0.0071	0.9758	0.0083

The ANOVA results are shown in Table 4. The model F-value of 77.53 implies the model is significant. There is only a 0.01% chance that an F-value this large could occur due to noise. The Lack of Fit F-value of 25.71 implies the lack of fit is significant. There is only a 1.22% chance that a lack of fit f-values this large could occur due to noise.

Table 4. Analyses of variance (ANOVA) for the quadratic model describing IBU adsorption onto Fe3O4/HNTs.

Source	Sum of squares	Df	Mean square	F-value	p-value
Model	83.31	5	16.66	77.53	< 0.0001
A-pH	66.40	1	66.40	308.97	< 0.0001
B-Fe_3O_4/HNTs	0.2091	1	0.2091	0.9728	0.3621
AB	0.0576	1	0.0576	0.2680	0.6232
A^2	16.62	1	16.62	77.32	0.0001
B^2	1.44	1	1.44	6.68	0.0415
Residual	1.29	6	0.2149	--	--
Lack of fit	1.24	3	0.4137	25.71	0.0122
Error	0.0483	3	0.0161	--	--
Corr total	84.60	11	--	--	--

The quadratic model equation that quantitatively describes the response's relationship with the factors was obtained. It can be used to determine the optimal experimental conditions for the absorption of IBU on Fe_3O_4/HNTs (Eq. 11).

$$IBU\ adsorbed\ (\%) = 3.47 - 3.33A + 0.1867\mathrm{B} - 0.12\mathrm{AB} + 2.5\,A^2 - 0.7338B^2 \quad (11)$$

According to equation 11, the main factor in the absorption of IBU on Fe_3O_4/HNTs is A (pH). At more acidic pH values, greater adsorption is obtained: at pH 2, approximately 8%; at neutral pH, around 3%; and at pH 12, it decreases between 2-2.5%. Also, a slight increase in adsorption is observed when the amount of Fe_3O_4/HNTs reaches a maximum. These results indicate that at acidic pH, the adsorption of IBU on Fe_3O_4/HNTs is favored because the protons of the carboxylic acid of the IBU form hydrogen bonds with the surface of the magnetite [64]. On the other hand, at basic pH, ibuprofen is in its anionic form due to the deprotonation of its carboxylic group, which presents a negative charge like the surface of Fe_3O_4/HNTs, repelling each other and disfavoring adsorption. Another significant value was B: Fe_3O_4/HNTs, the increase in adsorption with the rise in the amount of Fe_3O_4/HNTs is due to the increase in the number of active sites for the adsorption of the IBU. Figure 3 shows the response surface graph of IBU adsorption as a function of pH and the adsorbent dose.

 doi:10.20944/preprints202604.1141.v1

Finally, the optimal experimental conditions for the absorption of IBU were obtained at a concentration of 15 mg L^{-1}, a temperature of 298.15 K, a pH of 2, and a dose of Fe_3O_4/HNTs of 1.5 g L^{-1}, adsorbing an amount of 1.1 mg g^{-1} of adsorbent.

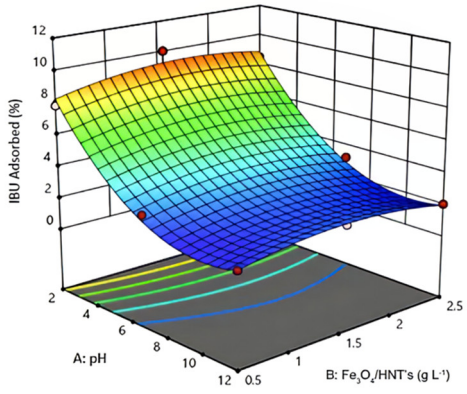

Figure 3. a) Response surface for the adsorption of IBU into Fe_3O_4/HNTs.

3.3. Adsorption Kinetics

Figure 4a shows that the adsorbed amount of IBU on Fe_3O_4/HNTs increased depending on the concentration. This increase, at higher concentrations of IBU, could be due to the shift of the adsorption-desorption equilibrium towards the adsorption process until the highest concentration was reached, which shows a saturation of the active sites of the adsorbent. To know the adsorption rate of IBU on the Fe_3O_4/HNTs adsorbate, adsorption kinetics, and equilibrium adsorption experiments were carried out, where data were obtained on the adsorbed amount of IBU per gram of adsorbent at 297.15 K as a function of time (pH 2 and dose of the adsorbent of 1.5 mg g^{-1}). The kinetic curves show adsorption behavior, where drug adsorption is slow in the initial days of contact with the adsorbent, followed by low gradual removal before reaching equilibrium. As can be seen in Figure 5, approximately 10% of the IBU was absorbed within the first five days, showing slow kinetics. In the following period, adsorption continues at lower rates, reaching equilibrium after 14 days. Based on the results of the regression coefficient, the pseudo-second-order equation is the model that best fits the adsorption of IBU on Fe, characteristic of adsorbents at low initial concentrations and with adsorbents with abundant active sites [65]. In this experiment, the adsorbent showed two stages: the first linear portion relates to the intra-particle diffusion of adsorbate on the sorbent surface, the fastest sorption stage, and the second stage (intra-particle diffusion) relates to the diffusion through smaller pores followed by equilibrium between the adsorbate and adsorbent.

FTIR spectra of the Fe_3O_4/HNTs and adsorbed Fe_3O_4/HNTs-IBU samples are presented in Figure 4b. FTIR spectra show the vibrations for HNTs in the range of 4000–400 cm^{-1}. The bands at 3695 and 3622 cm^{-1} correspond to the elongation of the HNTs structural O – H groups. The bands 3527, 3456, and 1650 cm^{-1} are due to the stretching and bending of the water molecules. The absorption bands found at 1091 cm^{-1} and 1032 cm^{-1} are due to the presence of Si – O – Si, and the band at 910 cm^{-1} corresponds to the bending of Al-O-OH, respectively, for HNTs [66]. Also, a vibration is observed at 553 cm^{-1} that corresponds to magnetite. It is essential to mention that magnetite presents this characteristic vibration in the infrared spectrum in the range of 540 to 570 cm^{-1} (Fe-O). The absence of IBU signal in the spectrum Fe_3O_4/HNTs-IBU indicates minimal IBU adsorption on the Fe_3O_4/HNTs surface.

 doi:10.20944/preprints202604.1141.v1

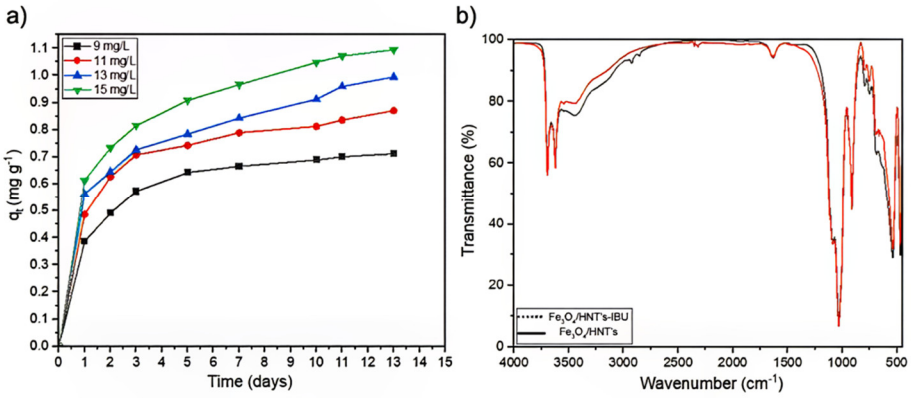

Figure 4. a) The amount of IBU adsorbed at a concentration of 15 mg L^{-1} on Fe_3O_4/HNTs as a function y b) IR for Fe_3O_4/HNTs and the adsorption of IBU on Fe_3O_4/HNTs.

Adsorption experiments were used to investigate the effect of contact time on IBU adsorption. To explain the adsorption of IBU on Fe_3O_4/HNTs, the PFO, PSO, and intraparticle diffusion equation models were used. Table 4 presents the fitting parameters of the kinetic models.

Based on the results of the regression coefficient, the PSO equation is the model that best fits the adsorption of IBU on Fe, characteristic of adsorbents at low initial concentrations and with adsorbents with abundant active sites. In this experiment, the adsorbent showed two stages, the first linear portion relates to the intra-particle diffusion of adsorbate on the sorbent surface, the fastest sorption stage, and the second stage (intra-particle diffusion) relates to the diffusion through smaller pores followed by equilibrium between the adsorbate and adsorbent. Table 5 presents the fitting parameters of the kinetic models. For 15 mg L^{-1}, k_2 is 3.276 E^{-4} (g·mg^{-1}·min^{-1}), with R^2 is 0.99872; pseudo-order kinetic models have been regularly obtained for the adsorption of IBU with other adsorbents such as graphene oxide nanoplatelets, doped copper, superparamagnetic silica nanocomposites, magnetic multi wall-carbon, and Fe_3O_4/Rice husk [65–70].

Table 5. Kinetic parameters values for the adsorption of IBU onto Fe_3O_4/HNTs.

Kinetic Model	R^2	Associated constants
PFO	0.97334	k_1 = 1.9711E^{-4} min^{-1}
PSO	0.99872	k_2 = 3.276E^{-4} g·mg^{-1}·min^{-1}
Intraparticle diffusion	0.99254	k_i = 0.00400 min^2 y C = 0.56147 mg g^{-1}

3.4. Adsorption Isotherms

The equilibrium experimental data on the adsorption of IBU from water (pH 7) are shown in Figure 5d-f together with fittings to the isotherm models considered. The parameters obtained for each model are shown in Table 6. The Langmuir model (R^2 = 0.87356) assumes monolayer adsorption on a structurally homogeneous support in addition to the fact that the sorption sites are energetically equivalent. However, Fe_3O_4/HNTs does not have a homogeneous surface since the magnetite is heterogeneously distributed on the surface of HNTs. So, these do not fit the type of adsorption of IBU on Fe_3O_4/HNTs. On the other hand, the Freundlich model (R^2 = 0.99126) had the best correlation. It assumes heterogeneous adsorption energies on the surface of an adsorbent. The parameter 1/n in the Freundlich equation reflects the degree of surface heterogeneity of the adsorbent. Lower values of 1/n (approaching zero) suggest greater surface heterogeneity, whereas values approaching one indicate a more homogeneous surface. It maintains low heterogeneity since the value of 1/n is close to 1, in congruence with Freundlich adsorption.

 doi:10.20944/preprints202604.1141.v1

Table 6. Isotherm parameters for adsorption of IBU on Fe_3O_4/HNTs.

Isotherm	R^2	Associated constants	
Henry	0.98837	K_H (mg L·mg^{-1}·g^{-1})	0.06783
Freundlich	0.99126	K_F (mg g^{-1})	0.12440
		(1/n)	0.83162
Langmuir	0.87356	K_L (L mg^{-1})	0.01970
		q_{max} (mg g^{-1})	5.14400

In Table 7, the adsorption capacity of IBU on Fe_3O_4/HNT is shown to be 5.144 mg L^{-1}, a very low value attributed to the weak hydrogen bonding interaction between IBU and the magnetite surface [64]. This result indicates that significant adsorption of IBU onto the HNTs does not occur. The minimal adsorption of IBU on Fe_3O_4/HNTs ensures that it remains available in the solution phase, thereby allowing the heterogeneous Fenton reaction to take place on the catalyst surface.

Table 7. Comparison of IBU adsorption in other clays and iron oxides.

Adsorbent	Experimental condition	Model kinetic	Adsorption Isotherm	Maximum adsorption capacity (mg g^{-1})	Reference
Fe_3O_4/Douglas fir biochar	60 min, pH 2-10, [IBU] = 100 mg L^{-1}	-	Langmuir	39.9	[64]
GO nanoplatelets	60 min, pH 2-10, [IBU] =100 mg L^{-1}	PSO	Langmuir	2.45-3.73	[65]
Magnetic multi wall-carbon nanotube	298 K, pH 4, [IBU] = 20 mg L^{-1}	PSO	Langmuir	1.15-11.8	[69]
Fe_3O_4/Rice husk	60 min, pH 7, $[IBU]_o$ == 4 mg L^{-1}	PSO	Langmuir	-	[70]
Kaolinite	298 K, pH 3, [IBU] = 60 mg L-1	-	-	3.1	[71]
Goethite	298 K, pH 3, [IBU] = 60 mg L^{-1}	-	-	6.1	[71]
Fe_3O_4/HNTs	30 min, pH 2, [IBU] =15 mg L^{-1}	PSO	Freundlich	5.144	This work

 doi:10.20944/preprints202604.1141.v1

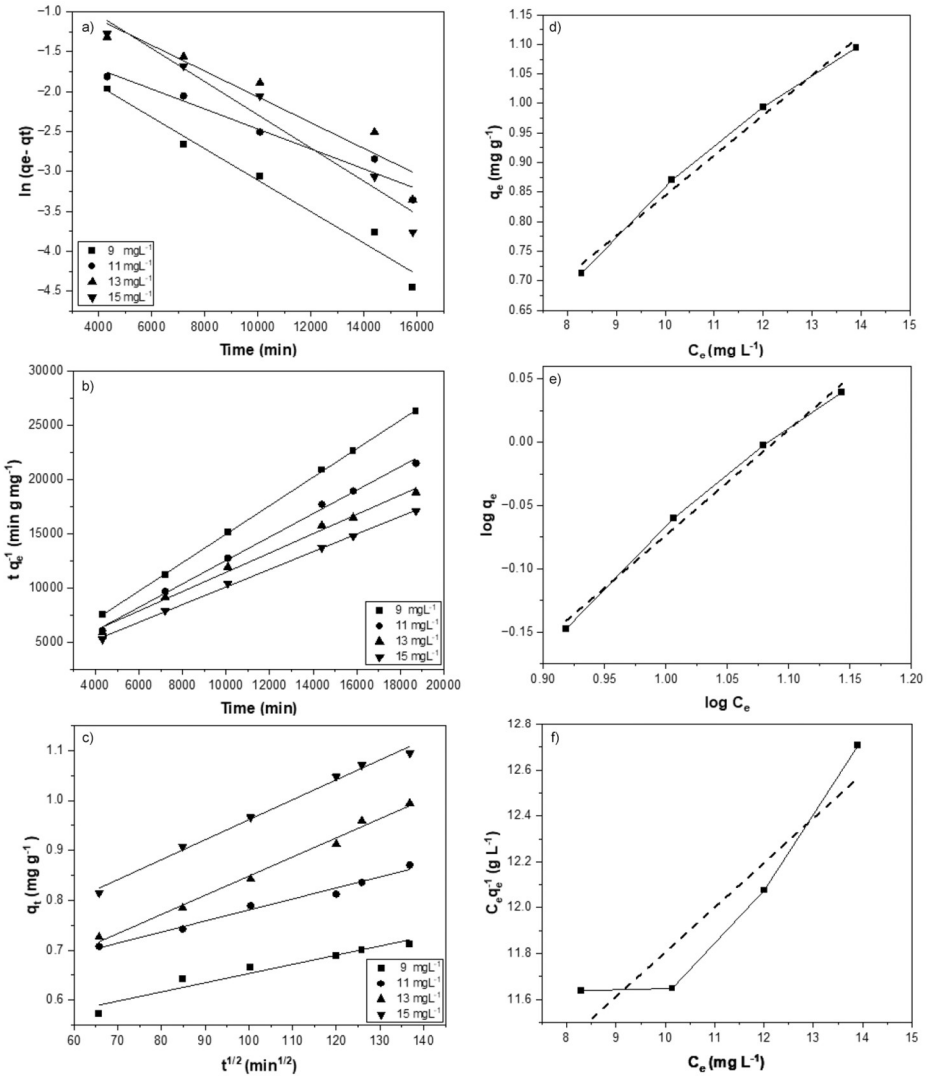

Figure 5. Kinetic model of a) pseudo-first order, b) pseudo-second order, and c) intraparticle diffusion, Isotherm of d) Henry, d) Freundlich, and f) Langmuir for the adsorption of IBU on Fe_3O_4/HNTs.

3.3. Ibuprofen Oxidation by Heterogeneous Fenton-Type Reaction (Monitoring)

A monitoring design was implemented to evaluate the factors used (A: pH, B: H_2O_2, and C: Fe_3O_3/HNT) and determine their effect on IBU degradation. Two levels were evaluated for each factor (-1 and +1) (Table 8). In addition to three center points, resulting in a total of 11 experiments where the percentage of oxidation was measured at each one (Table 9).

Table 8. Code and levels for monitoring design of oxidation of IBU on the Fe_3O_4/HNTs.

Factor	Code	Low level (-1)	Central point
pH	X1=A	2.0	7.0
H_2O_2 (M)	X2=B	0.5	1.5
Fe_3O_4/HNTs (g L^{-1})	X3=C	0.5	1.0

Table 9. Results obtained from the IBU mineralization monitoring design.

Run	H_2O_2 (M)	Fe_3O_4/HNTs (g L-1)	pH	Oxidation IBU (%)
1	0.050	0.5	2	85.69

 doi:10.20944/preprints202604.1141.v1

2	0.050	0.5	12	54.23
3	0.050	1.0	2	91.05
4	0.050	1.0	12	69.56
5	0.500	0.5	2	87.25
6	0.500	0.5	12	56.54
7	0.500	1.0	2	94.74
8	0.500	1.0	12	71.96
9	0.275	0.75	7	89.02
10	0.275	0.75	7	88.11
11	0.275	0.75	7	88.59

The statistical models, shown in Table 10, were obtained using the Design Expert 11 software. The quadratic model best fits for monitoring design of IBU mineralization with Fe_3O_4/HNTs.

Table 10. Lack-of-fit test of the optimization models for the oxidation of IBU onto Fe3O4/HNTs.

Source	Sequential p-value	Lack of fit p-value	Adjusted R^2	Predicted R^2
Linear	0.0009	0.0006	0.7401	0.6220
2FI	0.8766	0.0005	0.7085	0.4662
Quadratic	**0.0004**	**0.0122**	**0.9721**	**0.8767**
Cubic	0.3341	0.0071	0.9758	0.0083

Furthermore, using ANOVA (Table 11). The model F-value of 1177.02 implies the model is significant. There is only a 0.08% chance that an F-value this large could occur due to noise. P-values less than 0.0500 indicate model terms are significant. In this case A, B, C, AC, are significant model terms. Values greater than 0.1000 indicate the model terms are not significant. We can obtain an equation that quantitatively describes the relationship between the response and the factors, predict the amount of mineralized IBU, and generate a response surface plot.

Table 11. Analyses of variance (ANOVA) for the quadratic model describing IBU oxidation.

Source	Sum of squares	Df	Mean square	F-value	p-value
Model	1707.43	7	243.92	1177.02	0.0008
A-pH	1416.18	1	1416.18	6833.77	0.0001
B-H_2O_2	12.40	1	12.40	59.84	0.0163
C-Fe_3O_4/HNTs	237.62	1	237.62	1146.63	0.0009
AB	0.0365	1	0.0365	0.1759	0.7157
AC	40.05	1	40.05	193.27	0.0051
BC	0.6161	1	0.6161	2.97	0.2268
ABC	0.5202	1	0.5202	2.51	0.2540
Curvature	354.52	1	354.52	1565.96	0.0006
Pure Error	0.4145	2	0.2072	--	--
Cor Total	2032.36	10	--	--	--

$$IBU\ oxidation\ (\%) = 76.38 - 13.31A + 1.21B + 5.45C + 2.24AC + 0.2775BC - 0.2550ABC \quad (12)$$

According to equation 12 and Pareto chart (Figure 6), the variable with the main effect on mineralization is A: pH. With a t-value of 161.8.

 doi:10.20944/preprints202604.1141.v1

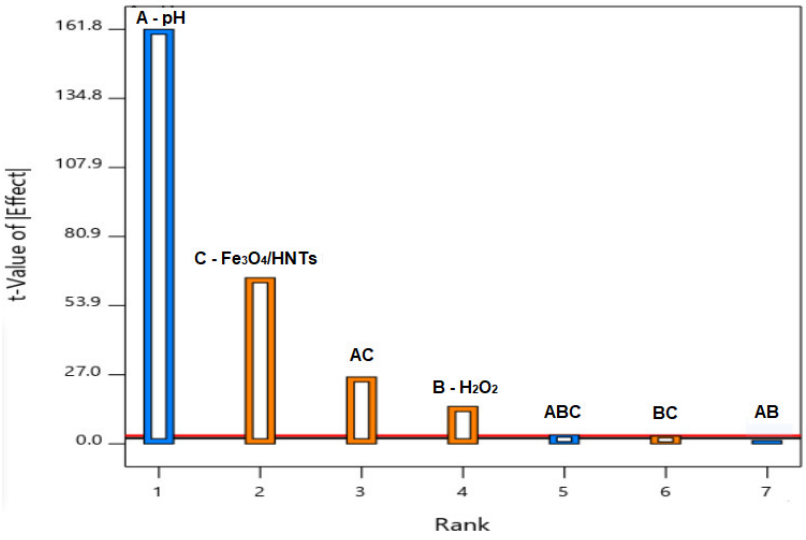

Figure 6. Pareto chart, which indicates the main effect on IBU mineralization where A: pH, B: H_2O_2, and C: Fe_3O_3/HNTs.

where low pH values favor the formation of hydroxyl radicals according to the following reaction:

$$Fe\ (ll) + H2O2 \rightarrow Fe\ (lll) + OH^{\circ} + OH^{-}$$

$$Fe\ (ll) + H2O2 + H^{+} \rightarrow Fe\ (lll) + OH^{\circ} + H2O$$

After pH, the variable with the greatest effect on IBU mineralization is C, the concentration of Fe_3O_3/HNTs. Hydroxyl radicals are formed on the surface of Fe_3O_3/HNTs when Fe reacts with hydrogen peroxide, thus forming hydroxyl radicals. Therefore, increasing the catalyst concentration increases the number of active sites available for hydroxyl radical formation. The next significant value was the AC (pH with Fe_3O_3/HNTs) interaction because pH affects the magnetite contained in the catalyst. The point zero charge (PZC) of magnetite is 6.5 so at acidic pH values the catalyst surface becomes protonated [72], favoring the adsorption of IBU onto Fe_3O_3/HNTs and thus degradation, since hydroxyl radicals are formed on the catalyst surface [73].

Finally, the variable with the smallest, but still significant, effect on IBU oxidation was the H_2O_2 concentration, since the hydroxyl radicals originate from hydrogen peroxide, so increasing the concentration favors degradation. The response surface plots obtained are shown in Figures 6 a), b), and c). The highest amount of IBU oxidation was 94.74% at pH 2, 0.5 M of H_2O_2, and 1 g L^{-1} of Fe_3O_3/HNT.

3.4. Ibuprofen Oxidation by Heterogeneous Fenton-Type Reaction (Optimization)

Once the effects of pH, Fe_3O_3/HNTs dosage, and H_2O_2 concentration on IBU degradation were determined, a Box-Behnken experimental design was implemented to find the optimal experimental conditions for IBU degradation through a Fenton-type heterogeneous reaction, maintaining a pH of 7 at a temperature of 298 K. The amounts of Fe_3O_3/HNTs and H_2O_2 were increased because, according to the monitoring design, a higher amount of Fe_3O_3/HNTs and H_2O_2 (Figure 6b) favors IBU degradation (Table 12). The results of the degradation of IBU are shown in Table 13.

Table 12. Code and levels of Box-Behnken design for degradation of IBU.

Factor	Code	Low level (-1)	Central point	Low level (+1)
H_2O_2	X1=A	0.25	0.5	0.75
Fe_3O_3/HNTs (g L-1)	X2=B	0.5	1.5	2.5

 doi:10.20944/preprints202604.1141.v1

Table 13. Degradation efficiency off IBU on Fe_3O_4/HNTs.

Run	Fe_3O_4/HNTs (g L-1)	pH	Adsorbed IBU (%)
Run	**H_2O_2 (M)**	**Fe_3O_4/HNTs (g L-1)**	**Mineralized IBU (%)**
1	0.25	0.5	87.34
2	0.25	1.5	94.48
3	0.25	2.5	89.42
4	0.50	0.5	89.23
5	0.50	1.5	99.99
6	0.50	1.5	99.98
7	0.50	1.5	97.21
8	0.50	1.5	98.84
9	0.50	2.5	90.47
10	0.75	0.5	91.57
11	0.75	1.5	98.06
12	0.75	2.5	89.34

The quadratic model offers the best fit, allowing us to identify the main factors and their interactions. Furthermore, using ANOVA, we can obtain an equation that quantitatively describes the relationship between the response and the factors, enabling us to predict the optimal amount of oxidation IBU.

Table 14. Lack-of-fit test of the optimization models for the oxidation of IBU onto Fe3O4/HNTs.

Source	Sequential p-value	Lack of fit p-value	Adjusted R^2	Predicted R^2
Linear	0.7970	0.0141	-0.1621	-0.7955
2FI	0.7379	0.0113	-0.2881	-2.6005
Quadratic	<0.0001	0.5212	0.9251	0.8204
Cubic	0.8415	0.2246	0.8969	-1.0033

The Model F-value of 28.16 implies the model is significant. There is only a 0.04% chance that an F-value this large could occur due to noise. P-values less than 0.0500 indicate model terms are significant. In this case A, B2 are significant model terms. Values greater than 0.1000 indicate the model terms are not significant. If there are many insignificant model terms (not counting those required to support hierarchy), model reduction may improve your model. The Lack of Fit F-value of 0.94 implies the lack of fit is not significant relative to the pure error. There is a 52.12% chance that a lack of fit f-value this large could occur due to noise. Non-significant lack of fit is good (Table 15).

 doi:10.20944/preprints202604.1141.v1

Table 15. Analysis of variance (ANOVA) for Box-Behnken experimental for the IBU oxidation with Fe3O4/HNTs.

Source	Sum of squares	Df	Mean square	F-value	p-value
Model	234.83	5	46.97	28.16	0.0004
A-H_2O_2	11.56	1	11.56	6.93	0.0389
B-Fe_3O_4/HNTs	0.4760	1	0.4760	0.2854	0.6124
AB	3.44	1	3.44	2.06	0.2009
A^2	6.07	1	6.07	3.64	0.1050
B^2	167.64	1	167.64	100.51	< 0.0001
Residual	10.01	6	1.67	--	--
Lack of fit	4.84	3	1.61	0.9356	0.5212
Pure Error	5.17	3	1.72	--	--
Corr total	244.84	11	--	--	--

$$\text{IBU oxidation (\%)} = 98.60 + 1.39A + 0.2817B - 0.9275AB - 1.51A^2 - 7.93B^2 \quad (13)$$

The quadratic model is the best fit, allowing one to know the main factors and their interactions. At pH 7, the catalyst dosage affects IBU mineralization, and the H_2O_2 concentration also significantly impacts IBU mineralization. This is because the hydroxyl radicals originate from hydrogen peroxide, so increasing its concentration promotes mineralization. The AB (Fe_3O_4/HNTs with H_2O_2) interaction also contributes, as it requires the reaction of H_2O_2 with Fe_3O_4/HNTs to form hydroxyl radicals. This equation holds true within the concentration range shown on the response surface in Figure 4d, where 99% degradation is achieved at a concentration of 1.5 g L^{-1} of Fe_3O_4/HNTs and 0.5 M H_2O_2.

 doi:10.20944/preprints202604.1141.v1

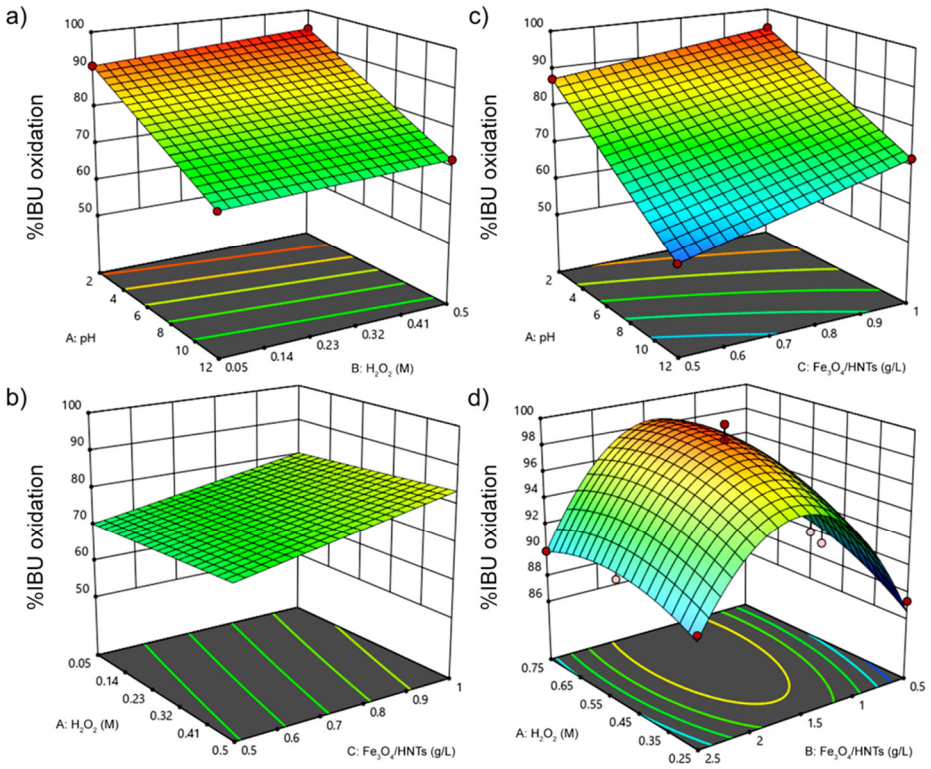

Figure 7. 3D Response surface graphs of the degradation of IBU in aqueous suspensions, with $[IBU]_0$ = 15 mg L^{-1} , temperature = 25 ± 1°C, held constant in all cases: a) dosage of [Fe_3O_4/HNTs] = 1 g L^{-1}; b) pH 7 and c) $[H_2O_2]_0$ = 500 mM; d).

3.4. Mineralization of Ibuprofen by Heterogeneous Fenton Reaction

Based on the results obtained in the experimental design for IBU oxidation, a heterogeneous Fenton reaction was carried out under the optimal reaction conditions: [IBU] = (15 mg L-1), Fe_3O_4/HNTs catalyst dosage (1.5 g L-1), pH 7[H_2O_2] = and a time of 24 hours, under which the highest IBU oxidation (99.99%) was obtained. The experiment was performed in triplicate.

Subsequently, the samples from the heterogeneous Fenton reaction were measured in duplicate, and the remaining concentration for each sample was obtained through the calibration curve and the mass spectra of the oxidation byproducts (Table 9).

The three systems achieved an IBU oxidation of close to 99%. Furthermore, only in one system was a signal corresponding to some byproduct formed in low concentrations during the oxidation of IBU observed.

Table 16. ibuprofen removed using a heterogeneous Fenton reaction.

System	IBU removed	Subproducts formed
1	99%	A (Time = 0.415 min)
2	99%	A (Time = 0.415 min)
3	99%	A (Time = 0.415 min) and B (1.24 min)

Table 17 presents advanced oxidation processes for the degradation and/or mineralization of IBU. Some of these processes are carried out under extreme pH conditions or require high energy. In

 doi:10.20944/preprints202604.1141.v1

this work, 99% degradation and 98% mineralization were achieved. Although the reaction time was long, the reaction conditions were mild.

Table 17. Performance comparison and reaction conditions of Fe_3O_4/HNT and other Fe-based catalyst.

Catalyst	Process	IBU Removed	Experimental Condition	Reference
Fe (ll)	Sonolysis and sono-Fenton	50%	pH (2.6 – 8.0), $[Fe^{2+}]$ = 10 mg L^{-1}, 3 hours	[35]
Fe(III)-gallic acid complex	Homogeneous modified Fenton-like oxidation	90.9%	Room temperature, [IBU]o = 0.05 M, [FeIII-GA complex] = 0.1 mM, pH 7.	[36]
Activated carbon fibers (ACFs) supported ferric citrate (Cit-Fe/ACFs)	Electro-Fenton	97%	120 min, current density of 7 mA cm^{-2}	[73]
Zero-valent iron	Electro-Fenton	92%	pH 6 , current density: 0.5 mA cm^{-2}, time 1 h, $[H_2O_2]$ in excess	[40]
Zero-valent iron (metallic Fe)	Electro-Fenton	80%	pH 6 , $[H_2O_2]$ = 50 µM, dosage ZVI 0.01 gL^{-1}	[40]
Fe-ordered mesoporous carbon (OMC)	Plasma-supported Fenton reactions	83%	[IBU] = 50 mg/L, $[H_2O_2]o$ = 43.3 mgL^{-1}, time = 2 h, $[H_2O_2]$ = 21.9 mgL^{-1}	[38]
Fe-zeolite	Plasma-supported Fenton	88%	Fe-zeolite= 1-5 gL^{-1} of 3 hours, “natural” pH conditions.	[35]
Fe/ZrO_2	Heterogeneous-Fenton	degradation (98%), mineralization (40%)	pH 5, 70 °C, pH 5, $[H_2O_2]$ (3%) 25 ml L^{-1}, [IBU] = 10 mg L^{-1}, 2 h	[75]
Fe/ZrO_2	Fenton-like process	80%	pH 3, 70 °C, pH 3, $[H_2O_2]$ = (3%) 30 ml L^{-1}, [IBU] = 10 mg L^{-1}, 2 h, Fe/ZrO_2= 400 mgL^{-1}	[76]
Iron-based MOF	Photo-Fenton	80%	[IBU] = 15 mg L^{-1}; $[Fe_3O_4]$ = 1.84 g L^{-1}; $[H_2O_2]$ = 600 mM; pH = 7.0; and temperature = 23 ± 2	[77]
Fe_3O_4	Heterogeneous Fenton-like oxidation	60%	$[H_2O_2]$ = 10 mM, Fe_3O_4 = 1 g L^{-1}, T=20°C, t = 3000 min, pH 7.0	[41]

 doi:10.20944/preprints202604.1141.v1

Fe_3O_4/clay slurry	heterogeneous Fenton-like oxidation	90%	[IBU] = 15 mg L^{-1} Fe_3O_4 = 2.0 g L^{-1}, [H_2O_2] = 600 mM; clay = 4.0 g L^{-1}; pH 7.0 and temperature = 23 ± 2°C	[42]
Carbon dots/Fe_3O_4@CS	Heterogeneous Fenton-like oxidation	90%	Persulfate = 5 mmol L^{-1}, [IBU] = 50 µmol Fe_3O_4@CS = 0.3 g L^{-1}, 2 h , temperature = 50°C	[43]
Humic acid coated magnetic particles	Heterogeneous photo-Fenton	80%	[H_2O_2] = 1.0 mmol L^{-1}, pH 3, 100 mg L^{-1} of Fe_3O_4/0.5HA, [IBU] = 0.2 mmolL^{-1}	[44]
Pd@Fe_3O_4	Sono-electrolytical Fenton	3-100%	[H_2O_2] = 3 mg L^{-1}: pH 3, 5.2 y 11 Pd@Fe_3O_4 = 0.1 gL^{-1}; [IBU] = 0.2 mgL^{-1}, t = 1h and temperature = 25°C	[45]
Fe_3O_4/MWCNTs	Heterogeneous Fenton-like oxidation	88.7%	pH 3; t = 20 h	[46]
Fe_3O_4/HNTs	Heterogeneous Fenton-like oxidation	Oxidation (99.99%), mineralization (99%)	pH 7.0, [IBU] = 15 mgL^{-1}, [H_2O_2] = 0.5 mol L^{-1}, Fe_3O_4 /HNTs = 1.5 gL^{-1}, temperature = 20°C, t = 24 h	This work

5. Conclusions

In this work, magnetite (Fe_3O_4) was synthesized in situ through the coprecipitation method on halloysite nanotubes (HNTs) to obtain an alternative method for eliminating ibuprofen, an emerging concern contaminant. SEM, XRD, FTIR, and BET characterized the nanoparticles obtained. The Fe_3O_4/HNTs was nearly spherical and uniform in size and exhibited irregular needles and agglomerations. The chemical composition by EDX confirms the presence of carbon, oxygen, silicon, aluminum, and sulfur elements in the catalyst. In XRD, it was possible to corroborate the formation of Fe_3O_4 on HNTs through diffraction patterns. The Fe_3O_4/HNTs sample has a multimodal pore size distribution of meso and macroporous material, an H1-type hysteresis cycle, and a surface area of 67.69 m^2g^{-1}.

Furthermore, the results fit pseudo-second-order kinetics, characteristic of adsorbents at low initial concentrations and with adsorbents with abundant active sites and a Freundlich adsorption, which assumes heterogeneous adsorption energies on the surface of an adsorbent isotherm. (R^2=0.99872, k_2 = 3.276E-4 y R^2=0.99126, K_F = 0.1244 mg g^{-1} respectively).

Finally, using the Design Expert 11 software, a Box Behnken-type experimental design. Through the ANOVA statistical analysis, it was found that the relationship of the response with the factors for

 doi:10.20944/preprints202604.1141.v1

the adsorption of IBU in Fe_3O_4/HNTs. was used, and the response surface and optimal experimental conditions for the mineralization of IBU (15 mg L^{-1}) at pH 7 and 298.15 K were obtained. These conditions are at a catalyst concentration (Fe_3O_4/HNTs) of 1.5 mg L^{-1} and an oxidant concentration (H_2O_2) of 0.5M, eliminating up to 99.99% of the aqueous medium. Fe_3O_4/HNTs nanoparticles are an efficient catalyst for oxidation and mineralization IBU in aqueous solution through a heterogeneous Fenton-like reaction.

Adsorption studies showed partial efficiency, while heterogeneous Fenton-type reactions achieved complete contaminant removal. This methodology offers the advantage of recovering the adsorbent/catalyst through a magnetic field. These results confirm the material's potential as an efficient alternative for treating water contaminated with IBU, helping to mitigate its environmental impact and health risks.

Author Contributions: Conceptualization, Y.M.V.R..; methodology, Y.M.V.R and E.A.G.G.; software, A.E.O.V.; validation, J.C.M.M; formal analysis, J.J.B. and J.A.C.C; investigation, E.A.G.G.; resources, X.X.; data curation, X.X.; writing—original draft preparation, E.A.G.G.; writing—review and editing, J.C.M.M..; visualization, X.X.; supervision, X.X.; project administration, A.E.O.V.; funding acquisition, Y.M.V.R. All authors have read and agreed to the published version of the manuscript." Please turn to the CRediT taxonomy for the term explanation. Authorship must be limited to those who have contributed substantially to the work reported.

Funding: This work was supported by Dirección General de Asuntos del Personal Académico DGAPA-PAPIIT (grant IN113722) and by Programa Interno de Cátedras de Investigación 2024, FES Cuautitlán-UNAM (grant CI2462). The APC was funded by Universidad Nacional Autónoma de México, and the awarded scholarship SECIHTI 1225471.

Acknowledgments: The authors have reviewed and edited the output and take full responsibility for the content of this publication.

Conflicts of Interest: The author(s) declared no potential conflicts of interest with respect to the research, authorship, and/or publication of this article.

References

1. Rout, P. R.; Zhang, T. C.; Bhunia, P.; Surampalli, R.Y. Treatment technologies for emerging contaminants in wastewater treatment plants: a review. *Sci. Total Environ.* **2021**, *753*, 141990. https://doi.org/10.1016/j.scitotenv.2020.141990
2. Rathi, B. S.; Kumar, P.S.; Show, P. L. A review on effective removal of emerging contaminants from aquatic systems: current trends and scope for further research. *J. Hazard. Mater.* **2021**, *409*, 124413. https://doi.org/10.1016/j.jhazmat.2020.124413
3. Morin-Crini, N.; Lichtfouse, E.; Liu, G.; Balaram, V.; Lado Ribeiro, A. R.; Lu, Z.; Stock, F.; Carmona, E.; Teixeira, M. R.; Picos-Corrales, L.A.; Moreno-Piraján, J. C.; Giraldo, L.; Li, C.; Pandey, A.; Hocquet, D.; Torri, G.; Crini, G. Worldwide cases of water pollution by emerging contaminants: a review. *Environ. Chem. Lett.* **2022**, *20* (4), 2311–2338. https://doi.org/10.1007/s10311-022-01447-4
4. Jiang, Y.; Ran, J.; Mao, K.; Yang, X.; Zhong, L.; Yang, C.; Feng, X.; Zhang, H. Recent progress in Fenton/Fenton-like reactions for the removal of antibiotics in aqueous environments. *Ecotoxicol. Environ. Saf.* **2022**, *236*, 113464. https://doi.org/10.1016/j.ecoenv.2022.113464
5. Kean, W. F.; Rainsford, K. D.; Buchanan, W. W. (2015). Chapter 6: Therapeutics of ibuprofen in rheumatic and other chronic and painful diseases. *Ibuprofen: Pharmacology, therapeutic uses and risks.* In K. D. Rainsford (Ed.); Wiley , 2015; pp. 237-312. https://doi.org/10.1002/9781118743614.ch6
6. Ahmed, H. R.; Kayani, K. F.; Ealias, A. M.; George, G**.** Biochar as an eco-friendly adsorbent for ibuprofen removal via adsorption: a review. *Inorg. Chem. Commun.* **2024**, *170*, 113397. https://doi.org/10.1016/j.inoche.2024.113397
7. Chopra, S.; Kumar, D. Ibuprofen as an emerging organic contaminant in environment, distribution and remediation. *Heliyon* **2020**, *6* (6), e04087. https://doi.org/10.1016/j.heliyon.2020.e04087

 doi:10.20944/preprints202604.1141.v1

8. He, R.; Wu, X.; Mu, H.; Chen, L.; Hu, H.; Wang, J.; ... Wu, B. Priority control sequence of 34 typical pollutants in effluents of Chinese wastewater treatment plants. *Water Res.* **2023**, *243*, 120338. https://doi.org/10.1016/j.watres.2023.120338
9. Březinova, T. D.; Vymazal, J.; Koželuh, M.; Kule, L. Occurrence and removal of ibuprofen and its metabolites in full-scale constructed wetlands treating municipal wastewater. *Ecol. Eng.* **2018**, *120*, 1–5. https://doi.org/10.1016/j.ecoleng.2018.05.020
10. Matamoros, V.; Bayona, J. M. Elimination of pharmaceuticals and personal care products in subsurface flow constructed wetlands. *Environ. Sci. Technol.* **2006**, *41*, 8171–8177. https://doi.org/10.1021/es0607741
11. Matamoros, V.; Garcia, J.; Bayona, J. M. Organic micropollutant removal in a full scale surface flow constructed wetland fed with secondary effluent. *Water Res.* **2008**, *42*, 653–660. https://doi.org/10.1016/j.watres.2007.08.016
12. Liu, Z. H.; Ma, Q. G.; Dai, L.; Dang, Z. Occurrence, removal and risk evaluation of ibuprofen and acetaminophen in municipal wastewater treatment plants: a critical review. *Sci. Total Environ.* **2023**, *891*, 164600. https://doi.org/10.1016/j.scitotenv.2023.164600
13. Khasawneh, O. F. S.; Palaniandy, P. Occurrence and removal of pharmaceuticals in wastewater treatment plants. *Process Saf. Environ. Prot.* **2021**, *150*, 532–556. https://doi.org/10.1016/j.psep.2021.04.045
14. Matamoros, V.; Hijosa, M.; Bayona, J. M. Assessment of the pharmaceutical active compounds removal in wastewater treatment systems at enantiomeric level. Ibuprofen and naproxen. *Chemosphere* **2009**, *75* (2), 200–205. https://doi.org/10.1016/j.chemosphere.2008.12.008
15. Zhang, Y.; Lv, T.; Carvalho, P. N.; Arias, C. A.; Chen, Z.; Brix, H**.** Removal of the pharmaceuticals ibuprofen and iohexol by four wetland plant species in hydroponic culture: plant uptake and microbial degradation. *Environ. Sci. Pollut. Res.* **2016**, *23* (3), 2890–2898. https://doi.org/10.1007/s11356-015-5552-x
16. Kahl, S.; Kleinsteuber, S.; Nivala, J.; van Afferden, M.; Reemtsma, T. Emerging biodegradation of the previously persistent artificial sweetener acesulfame in biological wastewater treatment. *Environ. Sci. Technol.* **2018**, *52* (5), 2717–2725. https://doi.org/10.1021/acs.est.7b05619
17. Gardner, M.; Jones, V.; Comber, S.; Scrimshaw, M. D.; Coello-Garcia, T.; Cartmell, E.; Ellor, B. Performance of UK wastewater treatment works with respect to trace contaminants. *Sci. Total Environ.* **2013**, *456*, 359–369. https://doi.org/10.1016/j.scitotenv.2013.03.088
18. Breitholtz, M.; Näslund, M.; Stråe, D.; Borg, H.; Grabic, R.; Fick, J. An evaluation of free water surface wetlands as tertiary sewage water treatment of micro-pollutants. *Ecotoxicol. Environ. Saf.* **2012**, *78*, 63–71. https://doi.org/10.1016/j.ecoenv.2011.11.014
19. Moeder, M.; Carranza-Diaz, O.; López-Angulo, G.; Vega-Aviña, R.; Chávez-Durán, F. A.; Jomaa, S.; Delgado-Vargas, F. Potential of vegetated ditches to manage organic pollutants derived from agricultural runoff and domestic sewage: a case study in Sinaloa (Mexico). *Sci. Total Environ.* **2017**, *598*, 1106–1115. https://doi.org/10.1016/j.scitotenv.2017.04.149
20. Morachis-Valdez, G.; Dublán-García, O.; López-Martínez, L. X.; Galar-Martínez, M.; Saucedo-Vence, K.; Gómez-Oliván, L. M. Chronic exposure to pollutants in Madín Reservoir (Mexico) alters oxidative stress status and flesh quality in the common carp *Cyprinus carpio*. *Environ. Sci. Pollut. Res.* **2015**, *22*, 9159–9172. https://doi.org/10.1007/s11356-014-4061-7
21. Amado-Piña, D.; Romero, R.; Salazar Carmona, E.; Ramírez-Serrano, A.; Gómez-Oliván, L. M.; Elizalde-Velázquez, G.; Natividad, R. Photo-Fenton treatment under UV and Vis light reduces pollution and toxicity in water from Madín Dam, Mexico. *Catalysts* **2024**, *14* (9), 620. https://doi.org/10.3390/catal14090620
22. Parolini, M.; Binelli, A.; Provini, A. Chronic effects induced by ibuprofen on the freshwater bivalve *Dreissena polymorpha*. *Ecotoxicol. Environ. Saf.* **2011**, *74* (6), 1586–1594. https://doi.org/10.1016/j.ecoenv.2011.04.025
23. Han, S.; Choi, K.; Kim, J.; Ji, K.; Kim, S.; Ahn, B.; Giesy, J. P. Endocrine disruption and consequences of chronic exposure to ibuprofen in Japanese medaka (*Oryzias latipes*) and freshwater cladocerans *Daphnia magna* and *Moina macrocopa*. *Aquat. Toxicol.* **2010**, *98* (3), 256–264. https://doi.org/10.1016/j.aquatox.2010.02.013

 doi:10.20944/preprints202604.1141.v1

24. Ding, T.; Yang, M.; Zhang, J.; Yang, B.; Lin, K.; Li, J.; Gan, J. Toxicity, degradation and metabolic fate of ibuprofen on freshwater diatom *Navicula* sp. *J. Hazard. Mater.* **2017**, *330*, 127–134. https://doi.org/10.1016/j.jhazmat.2017.02.004
25. Kim, S. H.; Nam, K. W.; Allam, B.; Choi, K.S.; Park, K. H.; Park, K.I. Quantification of the inflammatory responses to pro- and anti-inflammatory agents in Manila clam, *Ruditapes philippinarum*. *Fish Shellfish Immunol.* **2021**, *115*, 22–26. https://doi.org/10.1016/j.fsi.2021.05.019
26. Moro, I.; Matozzo, V.; Moschin, E.; Trentin, R.; Dalla Vecchia, F. Morpho-physiological responses by *Chlamydomonas reinhardtii* to different concentrations of ibuprofen. *Chem. Ecol.* **2021**, *37* (4), 352–368. https://doi.org/10.1080/02757540.2021.1886279
27. El-Sheikh, A. H.; Qawariq, R. F.; Abdelghani, J.I. Adsorption and magnetic solid-phase extraction of NSAIDs from pharmaceutical wastewater using magnetic carbon nanotubes: effect of sorbent dimensions, magnetite loading and competitive adsorption study. *Environ. Technol. Innov.* **2019**, *16*, 100496. https://doi.org/10.1016/j.eti.2019.100496
28. Kurczewska, J.; Cegłowski, M.; Schroeder, G. PAMAM-halloysite Dunino hybrid as an effective adsorbent of ibuprofen and naproxen from aqueous solutions. *Appl. Clay Sci.* **2020**, *190*, 105603. https://doi.org/10.1016/j.clay.2020.105603
29. Mohammadi-Aghdam, S.; Valinezhad-Saghezi, B.; Mortazavi, Y.; Qhoreishi, S. Modified Fe_3O_4/HAp magnetically nanoparticles as the carrier for ibuprofen: adsorption and release study. *Drug Res.* **2018**, *69* (2), 93–99. https://doi.org/10.1055/a-0647-1765
30. Feng, Y.; Long, Y.; Wang, Z.; Wang, X.; Shi, N.; Suo, N.; … Yu, Y**.** Performance and microbial community of an electric biological integration reactor (EBIR) for treatment of wastewater containing ibuprofen. *Bioresour. Technol.* **2019**, *274*, 447–458. https://doi.org/10.1016/j.biortech.2018.12.015
31. Khadir, A.; Motamedi, M.; Negarestani, M.; Sillanpää, M.; Sasani, M. Preparation of a nano bio-composite based on cellulosic biomass and conducting polymeric nanoparticles for ibuprofen removal: kinetics, isotherms, and energy site distribution. *Int. J. Biol. Macromol.* **2020**, *162*, 663–677. https://doi.org/10.1016/j.ijbiomac.2020.06.095
32. Munoz, M.; de Pedro, Z. M.; Casas, J. A.; Rodriguez, J.J. Preparation of magnetite-based catalysts and their application in heterogeneous Fenton oxidation–a review. *Appl. Catal. B Environ.* **2015**, *176*, 249–265. https://doi.org/10.1016/j.apcatb.2015.04.003
33. Usman, M.; Chaudhary, A.; Hanna, K. Efficient PFAS removal from contaminated soils through combined washing and adsorption in soil effluents. *J. Hazard. Mater.* **2024**, *476*, 135118. https://doi.org/10.1016/j.jhazmat.2024.135118
34. Gopinath, A.; Pisharody, L.; Popat, A.; Nidheesh, P. V. Supported catalysts for heterogeneous electro-Fenton processes: recent trends and future directions. *Curr. Opin. Solid State Mater. Sci.* **2022**, *26* (2), 100981. https://doi.org/10.1016/j.cossms.2022.100981
35. Adityosulindro, S.; Barthe, L.; González-Labrada, K.; Jáuregui Haza, U. J.; Delmas, H.; Julcour, C. Sonolysis and sono-Fenton oxidation for removal of ibuprofen in (waste)water. *Ultrason. Sonochem.* **2017**, *39*, 889–896. https://doi.org/10.1016/j.ultsonch.2017.06.008
36. Lekikot, B.; Mammeri, L.; Talbi, K.; Benssassi, M. E.; Abdessemed, A.; Sehili, T**.** Homogeneous modified Fenton-like oxidation using FeIII-gallic acid complex for ibuprofen degradation at neutral pH. *Desalination Water Treat.* **2021**, *234*, 147–157. https://doi.org/10.5004/dwt.2021.27626
37. Adityosulindro, S.; Julcour, C.; Barthe, L. Heterogeneous Fenton oxidation using Fe-ZSM5 catalyst for removal of ibuprofen in wastewater. *J. Environ. Chem. Eng.* **2018**, *6* (5), 5920–5928. https://doi.org/10.1016/j.jece.2018.09.007
38. Hirami, Y.; Hunge, Y. M.; Suzuki, N.; Rodríguez-González, V.; Kondo, T.; Yuasa, M.; Terashima, C. Enhanced degradation of ibuprofen using a combined treatment of plasma and Fenton reactions. *J. Colloid Interface Sci.* **2023**, *642*, 829–836. https://doi.org/10.1016/j.jcis.2023.02.136
39. Minella, M.; Bertinetti, S.; Hanna, K.; Minero, C.; Vione, D. Degradation of ibuprofen and phenol with a Fenton-like process triggered by zero-valent iron (ZVI-Fenton). *Environ. Res.* **2019**, *108750*, 1–8. https://doi.org/10.1016/j.envres.2019.108750

 doi:10.20944/preprints202604.1141.v1

40. Martone, L.; Minella, M.; Minero, C.; Sordello, F.; Vione, D. Effective degradation of ibuprofen through an electro-Fenton process, in the presence of zero-valent iron (ZVI-EF). *J. Clean. Prod.* **2022**, *367*, 132894. https://doi.org/10.1016/j.jclepro.2022.132894
41. Sabri, N.; Hanna, K.; Yargeau, V. Chemical oxidation of ibuprofen in the presence of iron species at near neutral pH. *Sci. Total Environ.* **2012**, *427*, 382–389. https://doi.org/10.1016/j.scitotenv.2012.04.034
42. Sun S. P.; Zeng X.; Lemley A. T. Nano-magnetite catalyzed heterogeneous Fenton-like degradation of emerging contaminants carbamazepine and ibuprofen in aqueous suspensions and montmorillonite clay slurries at neutral pH. *J. Mol. Catal. A: Chem.* **2013**, 371, 94–103. https://doi.org/10.1016/j.molcata.2013.01.027
43. Zhang, B. T.; Wang, Q.; Zhang, Y.; Teng, Y.; Fan, M. Degradation of ibuprofen in the carbon dots/Fe_3O_4@carbon sphere pomegranate-like composites activated persulfate system. *Sep. Purif. Technol.* **2020**, *242*, 116820. https://doi.org/10.1016/j.seppur.2020.116820
44. Gonçalves, N. P.; Minella, M.; Fabbri, D.; Calza, P.; Malitesta, C.; Mazzotta, E.; Prevot, A. B. Humic acid coated magnetic particles as highly efficient heterogeneous photo-Fenton materials for wastewater treatments. *Chem. Eng. J.* **2020**, *390*, 124619. https://doi.org/10.1016/j.cej.2020.124619
45. Thokchom, B.; Qiu, P.; Cui, M.; Park, B.; Pandit, A. B.; Khim, J. Magnetic Pd@Fe_3O_4 composite nanostructure as recoverable catalyst for sonoelectrohybrid degradation of ibuprofen. *Ultrason. Sonochem.* **2017**, *34*, 262–272. https://doi.org/10.1016/j.ultsonch.2016.05.030
46. Huaccallo-Aguilar, Y.; Diaz de Tuesta, J. L.; Álvarez-Torrellas, S.; Gomes, H. T.; Larriba, M.; Ovejero, G.; García, J. New insights on the removal of diclofenac and ibuprofen by CWPO using a magnetite-based catalyst in an up-flow fixed-bed reactor. *J. Environ. Manage.* **2021**, *281*, 111913. https://doi.org/10.1016/j.jenvman.2020.111913
47. Joussein, E.; Petit, S.; Churchman, J.; Theng, B.; Righi, D.; Delvaux, B. Halloysite clay minerals—A review. *Clay Miner.* **2005**, *40*(4), 383–426. https://doi.org/10.1180/0009855054040180
48. Vargas-Rodríguez, Y. M.; Obaya, A.; García-Petronilo, J. E.; Vargas-Rodríguez, G. I.; Gómez-Cortés, A.; Tavizón, G.; Chávez-Carvayar, J. A. Adsorption studies of aqueous solutions of methyl green for halloysite nanotubes: Kinetics, isotherms, and thermodynamic parameters. *Am. J. Nanomater.* **2021**, *9*(1), 1–11. https://doi.org/10.12691/ajn-9-1-1
49. Massaro, M.; Noto, R.; Riela, S. Past, present and future perspectives on halloysite clay mineral and catalyst supportals. *Molecules* **2020**, *25*(20), 4863. https://doi.org/10.3390/molecules25204863
50. Massaro, M.; Noto, R.; Riela, S. Halloysite nanotubes: Smart nanomaterials in catalysis. *Catalysts* **2022**, *12*, 149. https://doi.org/10.3390/catal12020149
51. Maleki T. S.; Sadati S.J. Synthesis and investigation of hyperthermia properties of Fe_3O_4/NTHs magnetic nanocomposite. *Inorg. Chem. Commun.* **2022**, 145, 110000. https://doi.org/10.1016/j.inoche.2022.110000
52. Revellame, E. D.; Fortela, D. L.; Hernandez, R.; Zappi, M. E.; Gang, D. D. A Critical Review on Kinetic Models and Isotherms for Adsorption-Based Water Treatment**.** *Cleaner Eng. Technol.* **2020**, *1*, 100032. https://doi.org/10.1016/j.clet.2020.100032
53. Ho, Y. S.; McKay, G. Pseudo-second order model for sorption processes. *Process Biochem.* **1999**, 34 (5), 451–465. https://doi.org/10.1016/S0032-9592(98)00112-5
54. Weber, W. J.; Morris, J. C. Intraparticle diffusion during the sorption of surfactants onto activated carbon. *J. Sanit. Eng. Div., Am. Soc. Civ. Eng.* **1963**, 89, 53–61. https://doi.org/10.1016/j.chemosphere.2022.136732
55. Foo, K. Y.; Hameed, B. H. Insights into the modeling of adsorption isotherm systems. *Chem. Eng. J.* **2010**, 156, 2–10. https://doi.org/10.1016/j.cej.2009.09.013
56. Freundlich, H. Über die Adsorption in Lösungen. *Z. Phys. Chem.* 1906, 57, 385–470.
57. Langmuir, I. The adsorption of gases on plane surfaces of glass, mica and platinum. *J. Am. Chem. Soc.* **1918**, 40 (9), 1361–1403. https://doi.org/10.1021/ja02242a004
58. Myers, R. H., Montgomery, D. C., & Anderson-Cook, C. M. (2016). Response surface methodology: process and product optimization using designed experiments. John Wiley & Sons.
59. Pierotti, R. A.; Rouquerol, J. Reporting physisorption data for gas/solid systems with special reference to the determination of surface area and porosity. *Pure Appl. Chem.* 1985, 57 (4), 603–619. https://doi.org/10.1351/pac198557040603

 doi:10.20944/preprints202604.1141.v1

60. Leofanti G.; Padovan M.; Tozzola G.; Venturelli B. Surface area and pore texture of catalysts. *Catal. Today* **1998**, 41, 207–219. https://doi.org/10.1016/S0920-5861(98)00050-9
61. Churchman G. J.; Davy T. J.; Aylmore L. A.; Gilkes R. J.; Self P. G. Characteristics of fine pores in some halloysites. *Clay Miner.* **1995**, 30(2), 89–98. https://doi.org/10.1180/claymin.1995.030.2.01
62. Brindley, G. W. Order-Disorder in the Clay Mineral Structures. In *Crystal Structures of Clay Minerals and Their X-ray Identification*; Brindley, G. W., Brown, G., Eds.; Mineralogical Society: London, 1980; pp 125–196. https://doi.org/10.1180/mono-5.2
63. Clark, C.; Downs, R. Using the American Mineralogist Crystal Structure Database in the Classroom. *J. Geosci. Educ.* **2004**, *52* (1), 76–80. https://doi.org/10.5408/1089-9995-52.1.76
64. Liyanage, A. S.; Canaday, S.; Pittman, C. U.; Mlsna, T. Rapid Remediation of Pharmaceuticals from Wastewater Using Magnetic Fe_3O_4/Douglas Fir Biochar Adsorbents. *Chemosphere* **2020**, *258*, 127336. https://doi.org/10.1016/j.chemosphere.2020.127336
65. Banerjee P.; Das P.; Zaman A.; Das P. Application of graphene oxide nanoplatelets for adsorption of ibuprofen from aqueous solutions: Evaluation of process kinetics and thermodynamics. *Process Saf. Environ. Prot.* **2016**, 101, 45–53. https://doi.org/10.1016/j.psep.2016.01.021
66. Yuan P.; Southon P. D.; Liu Z.; Kepert C.J. Organosilane functionalization of halloysite nanotubes for enhanced loading and controlled release. *Nanotechnology* **2012**, 23(37), 375705. https://doi.org/10.1088/0957-4484/23/37/375705
67. Xiong P.; Zhang H.; Li G.; Liao C.; Jiang G. Adsorption removal of ibuprofen and naproxen from aqueous solution with Cu-doped MIL-101(Fe). *Sci. Total Environ.* **2021**, 797, 149179. https://doi.org/10.1016/j.scitotenv.2021.149179
68. Kollarahithlu, C. S.; Balakrishnan R.M. Adsorption of pharmaceutical pollutants, ibuprofen, acetaminophen, and streptomycin from the aqueous phase using amine functionalized superparamagnetic silica nanocomposite. *J. Clean Prod.* **2021**, *294*, 126155. https://doi.org/10.1016/j.jclepro.2021.126155
69. Hanbali, G.; Jodeh, S.; Hamed, O.; Bol, R.; Khalaf, B.; Qdemat, A.; Samhan, S. Enhanced Ibuprofen Adsorption and Desorption on Synthesized Functionalized Magnetic Multiwall Carbon Nanotubes from Aqueous Solution. *Materials* **2020**, *13* (15), 3329. https://doi.org/10.3390/ma13153329
70. Adamu, H. I.; Faruruwa, M. D.; Adeyemi, M. M.; Tomori, W. B. Green Synthesized Iron Oxide Nanoparticles from Rice Husk for Ciprofloxacin and Ibuprofen Adsorption. *Afr. J. Adv. Sci. Technol. Res.* **2025**, *18*(1), 24–53. https://doi.org/10.62154/ajastr.2025.018.010673.
71. Behera, S. K.; Oh, S. Y.; Park, H. S. Sorptive Removal of Ibuprofen from Water Using Selected Soil Minerals and Activated Carbon. *Int. J. Environ. Sci. Technol.* **2012**, *9* (1), 85–94. https://doi.org/10.1007/s13762-011-0020-8.
72. Gamba, O. A., Badawi, M., Barres, O., Lainé, J., Mesquita, J., & Foucaud, Y. (2026). Influence of pH on the Surface Properties of Magnetite and Hematite: A Comprehensive Spectroscopic and Potentiometric Study. *Colloids and Surfaces A: Physicochemical and Engineering Aspects*, 139573. https://doi.org/10.1016/j.colsurfa.2026.139573
73. Jung, Y. S., Lim, W. T., Park, J. Y., & Kim, Y. H. (2009). Effect of pH on Fenton and Fenton-like oxidation. *Environmental Technology*, *30*(2), 183-190. https://doi.org/10.1080/09593330802468848
74. Liu, D.; Zhang H.; Wei Y.; Liu B.; Lin Y.; Li G.; Zhang F. Enhanced degradation of ibuprofen by heterogeneous electro-Fenton at circumneutral pH. *Chemosphere* **2018**, 209, 998–1006. https://doi.org/10.1016/j.chemosphere.2018.06.164
75. Hussain S.; Aneggi E.; Briguglio S.; Mattiussi M.; Gelao V.; Cabras I.; ... Goi D**.** Enhanced ibuprofen removal by heterogeneous-Fenton process over Cu/ZrO_2 and Fe/ZrO_2 catalysts. *J. Environ. Chem. Eng.* **2020**, 8(1), 103586. https://doi.org/10.1016/j.jece.2019.103586
76. Hussain S.; Aneggi E.; Trovarelli A.; Goi D**.** Heterogeneous Fenton-like oxidation of ibuprofen over zirconia-supported iron and copper catalysts: Effect of process variables. *J. Water Process Eng.* **2021**, 44, 102343. https://doi.org/10.1016/j.jwpe.2021.102343
77. Sun S.; Hu Y.; Xu M.; Cheng F.; Zhang H.; Li Z. Photo-Fenton degradation of carbamazepine and ibuprofen by iron-based metal-organic framework under alkaline condition. *J. Hazard Mater.* **2022**, 424, 127698. https://doi.org/10.1016/j.jhazmat.2021.127698

 doi:10.20944/preprints202604.1141.v1